I.J. Image, Graphics and Signal Processing, **2024, 4, 87-105**
Published Online on August 8, 2024 by MECS Press (http://www.mecs-press.org/)
DOI: 10.5815/ijigsp.2024.04.07

Computerized Acute Myeloid Leukemia Classification Using Hybrid Dilated DenseSqueeze Network from Peripheral B Stain Analysis

Krishna Prasad Palli*
Vasireddy Venkatadri Institute of Technology, Jawaharlal Nehru Technological University, Namburu, Andhra Pradesh, 522508, India
Email: prkrishnaprasad@vvit.net
ORCID iD: https://orcid.org/0000-0003-0541-8919
*Corresponding Author

Edara Sreenivasa Reddy
University College of Engineering, Acharya Nagarjuna University, Nagarjuna Nagar, Guntur, Andhra Pradesh, 522510, India
Email: edara_67@yahoo.com
ORCID iD: https://orcid.org/ 0000-0001-7347-2680

Chandra Sekharaiah K.
University College of Engineering, Jawaharlal Nehru Technological University, Hyderabad, Telangana, 500085, India
Email: chandrasekharaiahk@gmail.com
ORCID iD: https://orcid.org/0000-0001-5102-1408

Received: 02 December, 2023; Revised: 18 January, 2024; Accepted: 22 February, 2024; Published: 08 August, 2024

Abstract: In medical diagnosis, Artificial Intelligence (AI) has offered significant revolution, especially for cancers. Acute Myeloid Leukemia (AML) is a deadly blood cancer caused by the rapid growth of abnormal White Blood Cells (WBCs) in humans. Although AML classification is a popular area of research, existing detection methods utilize manual examination of microscopic blood samples, which includes high complexity and tedious. Therefore, this work presented a computerized deep learning model-based AML classification from peripheral blood stain images, which helps in earlier AML diagnosis. The processing steps followed in AML classification are Image Pre-processing, Localization of RoI (Region of Interest), Fusion-based Feature Extraction and Classification. First, the input image is pre-processed, which includes noise filtering, image resizing, and colour conversion. The noise in the image is filtered using normalized Gaussian filtering (NGF). Next, the image is resized into a standard size, and the RGB image is converted into CMYK colour space. Then, the RoI is identified using the Image Moment Localization (IML) technique. Next, the valuable multi-level dense features are extracted using DenseSqueeze Network, and multi-scale features are extracted using Dilated Convolution Spatial Pyramid Pooling (Dilated CSPP). Both these extracted features are fused using the element-wise summation. Finally, the Softmax classifier is used in the last layer to classify the classes of AML and the loss in the network is optimized using the Improved Artificial Fish Swarm (Improved AFS) algorithm. The proposed work results in 99% of accuracy, 98.5% of precision and 98.9% of F-score by using the AML-Cytomorphology LMU dataset.

Index Terms: Gaussian Filtering, Moment Localization, Softmax, Artificial Fish Swarm algorithm, Convolution Spatial Pyramid Pooling, Dilated CSPP

1. Introduction

White blood cells (WBCs) are analyzed to detect leukaemia; it is a type of cancer which consists of two types: Acute and chronic leukaemia. The cancer is obtained in the white blood cells of human beings [1]. Myeloid and

lymphoid cells are the cancer cells based on myeloblastic and lymphocytic, respectively. The primary etiology of Acute Myeloid Leukemia, also known as AM Leukemia (AML), is the excessive generation of young white blood cells [2]. According to a report by the World Health Organization (WHO), an estimated 0.02 million new cases of AML will be diagnosed in 2018. The estimated number of AML-related fatalities in India in 2018 is 10,670, with an approximate annual incidence of 75,000 new cases. In order to reduce the mortality rate year by year, early detection is urgently needed to identify the growth stage of AML cells in the human body [3]. To identify the diseases, microscopic images are helpful to detect the disease in the blood. There are three main components of blood: WBC (leukocytes), platelets and RBC (erythrocytes) [4].

Chronic leukemia is characterized by an abnormal white blood cell count and impaired functionality compared to healthy white blood cells. This may progress from normal to abnormal over time if the disease is not detected sooner. This has the potential to induce severe harm to patients' health [5,6]. In the initial stages, the disease spreads throughout the human body and manifests itself in the bone marrow. In a healthier person, the growth of white blood cells mainly depends on the growth of the body, but leukaemia disease can occur abnormally in the human body [7].

Normally, the dark purple colour of leukaemia cells is easier for detecting the disease, but the processing and assessment make it difficult to identify the texture and pattern-based variations [8, 9]. It can be recognized by the shape and size of platelets and red blood cells. Due to the age limit of more than 7–8 years, the patient's age plays a decisive factor in the prognosis [10]. The probability range of the disease can decrease up to 20 years, and begin to increase the age limit to around 50 years. Morphology is the primary diagnostic tool employed in the medical profession for acute lymphoblastic leukemia [11]. Using this diagnostic tool, when a patient has acute lymphoblastic leukaemia, they have a certain amount of cancer cells in the bone marrow [12,13]. Diagnosis of acute lymphoblastic leukaemia involves accurately distinguishing the cancer cells from normal cells. The classification of leukaemia is mainly into M0 to M7 based on immunophenotypic, morphological criteria and cytochemical discoveries. M0 represents lower disease severity, and M7 represents high disease severity. For cancer cell prediction, the normal cells look similar to the cancer cells in microscopic images [14]. It is difficult to distinguish both cells in the microscopic images. Consequently, precise disease analysis is essential for the diagnosis of leukemia [15].

To overcome such challenges, deep learning models (or machine learning models) are incorporated into the microscopic image to analyze AML. There are several research studies on leukaemia cancer detection [16]. Based on the use of traditional machine learning techniques, features of leukaemia cells are extracted, and then the classification process is performed [17]. The medical field makes extensive use of deep learning techniques as opposed to machine learning processes. Deep learning models help solve numerous problems and challenges in image analysis based on automation processes [18]. Nowadays, automated diagnosis is urgently needed for the identification of multiple diseases and to employ automated feature engineering. In computer vision technology, microscopic image segmentation and recognition are essential to the deep learning process [19]. The most commonly used neural network is the Convolutional Neural (CN) network. It has a high degree of adaptability, self-learning ability and generalization ability for medical imaging problems [20]. This research article applies an effective deep-learning model to identify leukaemia diseases using image-modal microscopic blood samples. This enables the wide distribution in which the channel-wise features are used by the lower layers. Furthermore, this model helps to improve feature discriminability between normal and affected cells.

1.1 Motivation

The automatic detection of disease analysis saves health professionals' time and reduces the time consumed by manual picture data examination. Various disease detection methods are used in healthcare to obtain accurate disease classification. In addition, AML is used in the human body to protect patients from bone marrow or bone cancer and to prevent serious health problems. Nowadays, much research is being carried out to detect leukocyte diseases effectively. However, due to the similarity between normal cells and leukaemia cells, there is an urgent need for an effective model to identify patients' blood cells accurately. Therefore, this work presents a new computer-based hybrid network for assessing AML from peripheral blood spot images. The following describes the primary contribution of the proposed work:

- To perform Image Moment Localization based RoI extraction and generate a semantic segmentation model to assist the diagnosticians in localizing WBCs and to increase the diagnosis accuracy.
- To introduce Feature Extraction using DenseSqueeze Network and Dilated Convolution Spatial Pyramid Pooling (Dilated CSPP) to extract the multi-level dense features and multi-scale features, respectively.
- To fuse the extracted features using element-wise summation, the Softmax classifier is used in the last layer to classify the classes of AML.
- To optimize the loss in the network using the Improved Artificial Fish Swarm (Improved AFS) algorithm.

In this paper, five different sections are organized. 1. Introduction that gives the basic information about the technologies. 2. Various related works of classification methods are described. 3. The proposed methodology for AML classification of peripheral blood stain images using deep learning methodology is described in detail. 4. The result and discussion are described in the section. 5. Overall conclusion, future work and references are given in this section.

2. Related Works

This section describes various surveys related to AML classification using deep learning.

Alagu S et al. (2021) [21] implemented the detection of acute myeloid (AM) leukaemia using a computer-aided classification framework in blood smear images. AML detection manually was time-consuming and challenging due to the need for precise output in peripheral blood stain images. In this paper, computer-assisted classification is suggested as a method for identifying alterations in the nucleus of myeloma cells within microscopic images. To obtain the cell nucleus and cell mask, the pre-processing and segmentation operations were used. To better identify AML, the nuclear shape was irregular and the image texture was also changed. A total of 260 images from the database of the University of Isfahan were considered as blood smear images for training and testing purposes. By employing this methodology, the K-means clustering algorithm was utilized to partition the cytoplasm and nucleus. Image classification was determined using a random forest classifier. The accuracy of this model was achieved at 95.89%.

Yoshifuji et al. (2021) [22] introduced acute myeloid leukemia-based CT classification of lung images. Computed tomography (CT) images of the chest were considered for 435 patients with AML and for 20 patients with pulmonary leukemic (PL) infiltration, which were categorized into four patterns. The CT findings were obtained for the values 35%, 20%, 35%, and 10% for types A, B, C, and D, respectively.

Sha. K et al. (2021) [23] implemented acute myeloid leukaemia detection based on a novel 5-gene signature prediction method. The identification of genes associated with prognosis was facilitated by Kaplan-Meier. The Cancer Genome Atlas (TCGA) dataset was used to collect information on 173 clinical AML data and validated by the Oregon Health and Science University dataset. In this model, unsupervised hierarchical clustering was established for the classification of AML such as LRCH4, FCHO2, PLA2G4A, DOCK1 and CALCRL expression levels. The ROC curve results were obtained for the TCGA dataset at about 0.74.

Bukhari et al. (2022) [24] applied leukaemia cancer detection using a squeeze and excitation-based deep learning framework in microscopic blood samples. By applying a novel iteration of the deep learning algorithm, the microscopic images of blood samples were analyzed. Integration of recalibration of channel-wise feature representation was achieved via squeeze-and-excitation learning. The efficacy of leukemia diagnosis through the utilization of microscopic images and patient blood samples was enhanced by this model. The dataset used for blood samples from leukaemia patients such as ALL_IDB1 and ALL_IDBI2. Using this method, accuracy rate results for squeeze and excitation-based convolutional neural (CN) networks of 100% and 99.98% were achieved for ALL_IDB1 and ALL_IDB2, respectively.

Acute lymphoblastic leukemia diagnosis was implemented by Granero et al. (2021) [25] using a quaternion-valued convolutional neural network. This model applied the quaternion-valued parameters to capture and generalize the multidimensional data. The CN network was utilized to classify lymphoblasts in accordance with the microscopically observed blood stain images. The dataset was obtained from the ALL-IDB dataset. The colour image was extracted with fewer parameters. In comparison to the real-valued model, the quaternion-evaluated convolutional neural (CN) network accomplished approximately 34% of the parameters.

Table 1. Survey on existing methodologies

Author Name& Reference	Techniques	Dataset	Limitation	Performance
Alagu S et al. [21]	Random forest	Microscopic images	Limited features	Accuracy- 95.89%
Yoshifuji et al. [22]	Edema-like opacities	clinical data	Simple and basic methods can used	CT findings were obtained for the values of 35%, 20%, 35% and 10% for types A, B, C and D, respectively.
Sha. K et al. [23]	Kaplan–Meier and multivariate analyses	TCGA	Less performance	ROC curve was obtained about 0.74
Bukhari et al.[24]	CNN	ALL-IDB1 and ALL-IDB2	It isn't useful for different types of acute lymphocytic leukaemia	Accuracy-100%, 99.98% for ALL_IDB1 and ALL_IDB2, respectively.
Granero et al. [25]	CNN	ALL-IDB	Limited features	Quaternion value-34%
Boldu et al. [26]	CNN	EDTA	High complex model	Sensitivity specificity for myeloid leukaemia is 92.30% to 93.70%, and sensitivity specificity for lymphoid leukaemia is 89% and 100%.

Boldu et al. (2021) [26] obtained the diagnosis of acute leukaemia lineage using a deep learning model (ALNet) in peripheral blood cell images. Identifying morphological differentiation in blood cells is difficult. This method provided artificial intelligence-based analysis to predict acute leukaemia based on blood cell images. A total of 16,450 single-cell images were analyzed for values of 85% and 15% for training and test sets, respectively. ALNet was involved in the study of samples from all patients with myeloid leukaemia and promyelocytes. The blood sample images were collected from Ethylenediaminetetraacetic acid (EDTA) using the SP10i slide stainer. The blood cells were recorded using the

CellaVisionDM96 based on digital images. The results evaluated for myeloid leukaemia are based on the values of 100%, 92.30% and 93.70% for sensitivity, specificity and precision, respectively. In lymphocytic leukaemia, however, results of 89% and 100% were achieved for sensitivity and specificity, respectively. Table 1 shows the survey on existing methods.

The survey of current approaches reveals certain shortcomings, including reduced performance, reduced feature learning ability, and limited features. As a result, the total system performance was low. To address the problems of existing models and increase system performance, a novel approach was developed in this research. In this research, a novel technique for classifying AML was proposed.

3. Proposed Methodology

This paper presents a computational deep-learning model for AML classification using peripheral blood stain images. The processing steps followed in AML classification are image pre-processing, RoI (Region of Interest) localization, fusion-based feature extraction and classification. First, the input image is pre-processed, which includes noise filtering, image resizing, and colour conversion. The noise in the image is filtered using normalized Gaussian filtering (NGF). Fig 1 shows the architecture of the proposed model.

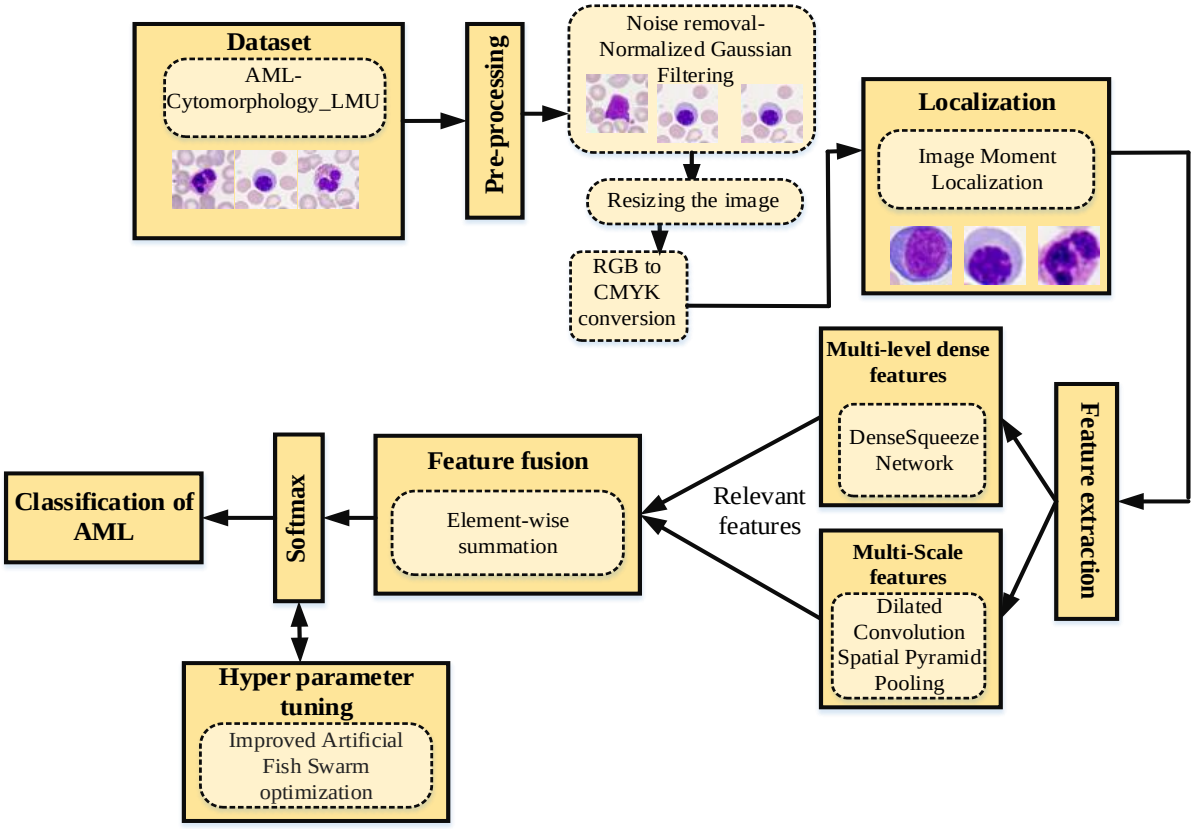

Fig. 1. Workflow Architecture of the proposed model

It then resizes the image to a standard size and converts the RGB image to the CMYK colour space. The RoI is then identified using the Image Moment Localization (IML) technique. Next, the valuable multi-level dense features are extracted using the DenseSqueeze network, and the multi-scale features are extracted using Dilated Convolution Spatial Pyramid Pooling (Dilated CSPP). These two extracted features are merged using element-wise summation. Finally, the softmax classifier is used in the last layer to classify the AML classes and the loss in the network is optimized using the Improved Artificial Fish Swarm (Improved AFS) algorithm. Compare to existing AML classification techniques our proposed method obtained high results. The novelty of proposed approach: Perform accurate AML classification and produce superior results, the proposed approach used three pre-processing techniques compare to single contribution model proposed three pre-processing techniques make a help in producing compactable results, here in feature extraction stage multi-level dense features are extracted using DenseSqueeze network combine the advantage of dense and squeeze network, squeeze network contain dilated convolutional layer instead of convolutional layer, dilated convolutional layer help to produce less number of parameter model, in Improved AFS the best solution is chosen based on optimization technique to tuning hyper parameter and this tends to reduce feature dimensionality issues and overall processing time.

3.1 Pre-processing

The input image is pre-processed, which includes noise filtering, image resizing and colour conversion.

3.1.1. Normalized Gaussian Filtering

Proposed approach used NGF [27] to smooth and remove image noise more efficiently. When this filter is applied to an image, it works in two stages.

Step 1: In the first stage, the center position of the image is filtered after multiplying the weight of the image by all pixel values to produce the new pixel values.

Step 2: The final image is created in the second step by vertically filtering all pixels of the horizontally processed image.

The mathematical expression for the NGF is denoted as follows,

$$G(I) = \frac{\frac{1}{\sqrt{2\pi\omega^2}} e^{-(I-\upsilon)^2}}{\left(2\omega^2\right)} \tag{1}$$

Here $G(I)$ denotes the probability density function for NGF; the grey level image is denoted by I, the mean value represented as υ, ω represented as standard deviation. The Gaussian filter's standard deviation (ω) produces a normalized image. Compared to other filtering techniques proposed NGF provide more benefits in pre-processing of images such as reduce bright pixels, smooth out the edges, reduce noise from the image taken in low light and provide compactable results in classification of AML. Proposed NGF takes less time to remove the unwanted noises in input image and image smoothing.

3.1.2 Image resizing using CMYK

The initial image (400, 400, 4) in the RGB scale converts to the CMYK scale (100, 100, 3) because leukocytes have no yellow component and are completely black when viewed through a yellow component. Benefits of using CMYK is, it works well with high-graphics or photographic images with a lot of colour depth. CMYK is the best technique to attain accurate viewing images on a printed piece.

3.1.3 Image Moment Localization

In this phase, the RoI is identified using IML [28] to find the objects in the image and draw the bounding box around the image. Following the extraction of the WBC nucleus from the channel via the Otsu thresholding method, a binary mask was generated. Following that, isolated apparatuses were eliminated using post-processing operations, and an advanced binary mask was generated by employing morphological introductory and maximum connected region (MCR) techniques. Then, by utilizing image moments, the centroid of the nucleus is ascertained. The mathematical expression for detecting the nucleus' centroid can be expressed as follows.

$$M_{pq} = \sum_{u}\sum_{v} u^{p} v^{q} I(u,v) \tag{2}$$

$$CH_{u} = \frac{M_{10}}{M_{00}} \tag{3}$$

$$CH_{v} = \frac{M_{01}}{M_{00}} \tag{4}$$

Where $I(u,v)$ denotes the intensity of the image, CH_u and CH_v are denoted as the channel of the u and v coordinates, respectively. M_{pq} denotes the maximum diameter of the WBCs. Pixels inside the RoI are set to 1 and those outside the RoI are set to 0 in the mask image. RoI makes a boundaries to identify disease portions on the image.

3.2 Feature extraction

The proposed method used two feature extraction techniques, DenseSqueeze Network and Dilated Convolution Spatial Pyramid Pooling, to extract relevant multi-level dense features and multi-level scaling features.

3.2.1 DenseSqueeze Network

DenseSqueeze Network used to extract multi-level dense features in the image. DenseNet reduces the parameters of Resnet by half while improving model performance. The inputs of each DenseNet layer concatenate data from all

previous layers, intensively attached the outputs of these layers, and practice the feature reprocess function by integration features on the channel. In order to prevent excessive increases the number of parameters, the DenseNet uses growth rate to limit amount of feature records produced by each layer. In DenseNet, it is relaxed to pass false information directly to previous layers thus the final classification layer can openly monitor these layers [29]. In addition, it can stop convergence during training of the neural network and solve the vanishing gradient problems. Fig 2 shows the architecture of the DenseSqueeze network.

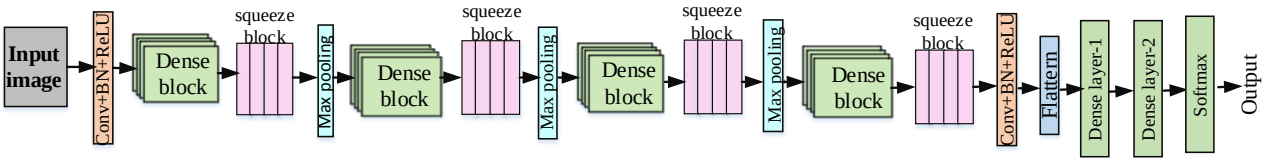

Fig. 2. Architecture of DenseSqueeze Network

Proposed DenseSqueeze network includes 22 convolutional layers with a rectified linear unit (ReLU) activation function, 22 batch normalization layers, four concatenation layers, four additional layers, three max-pooling layers, a flattened layer, and six dense layers for extracting multi-level dense features. DenseSqueeze architecture contains four dense blocks and squeeze blocks with different numbers of convolutional layers. In order to reduce computational power and improve model performance, the pooling layer helps extract only the dominant features. The DenseNet and Squeeze Net architecture that inspired the concepts of dense and squeeze blocks. Fig 3 shows architecture of dense block.

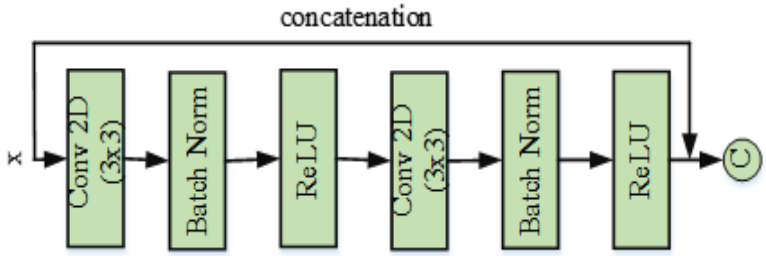

Fig. 3. Architecture of Dense block

A type of convolutional neural network called DenseNet makes use of dense connections between various layers in a feed-forward manner. Additionally, it promotes feature reuse. Similarly, Squeeze Net is a CNN type that has a good degree of accuracy and a smaller architecture. Through channel correlation, which can rise sensitivity to feature material, Squeeze Block improves the learning of convolutional features. Fig 4 shows the architecture of the Squeeze block.

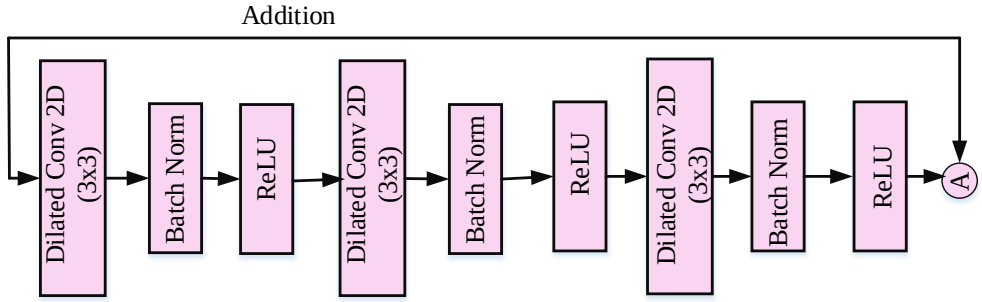

Fig. 4. Architecture of Squeeze block

Compare to traditional Squeeze network the proposed model used dilated convolutional block instead of normal convolutional block. Adding dilated convolutional layer instead of convolutional layer is one of the novelty in proposed work. Dilated convolutional layer reduce the number of parameter of the proposed model. The Squeeze process compresses the global average pooling to produce the global average Receptive Field, which is subsequently utilized to determine the feature map's weight and amplify the important features while attenuating the unimportant ones. Next, all of the data from the squeeze is output for excitation process. To determine the nonlinear interaction among the channels, nonlinear relationship between them is first learned using the Softmax activation function. Two completely associated layers are designed around the nonlinearity to integrate feature map data in each channel, thereby reducing number of

channels and creating a bottleneck by minimizing the processing overhead. DenseSqueeze Network effectively extracts multi-level dense features.

3.2.2 Dilated Convolution Spatial Pyramid Pooling

Proposed model used dilated CSPP model for extracting multi-level scale features. Dilated convolution, also named as atrous convolution, can exponentially growth the receptive area lacking reducing the spatial dimension. The dilated convolution can enlarge the convolution kernel's receiving field. Multi-scale setting data is obtained via dilated CSPP [30], and upsampling is employed to directly retrieve the prediction results. Backpropagation helps the filters in the convolutional layer learn by providing information about their weights after each iteration, hence minimizing the loss of expected output. Each Conv block CNN-SPP consists of two convolutions with $L=4$ layers of convolution. To reduce computational complexity, max pooling is applied to feature maps of $L-th$ convolutional layer of conv-block 1.

$$\hat{u}^{(l)} = \frac{u^{(l)} - E\left[u^{(l)}\right]}{\sqrt{Var\left[u^{(l)}\right]}} \tag{5}$$

Here $u^{(k)}$ represents the particular activation, $E\left[u^{(l)}\right]=\frac{1}{k}\sum_{x=1}^{k} u_x^{(l)}$ and $\sqrt{Var\left[u^{(l)}\right]}=\frac{1}{k}\sum_{x=1}^{k}\left(u_x^{(k)}-E\left[u^{(l)}\right]\right)^2+\in$. Here $\in= 0.001$ is provided in the calculation for numerical constancy by confirming $\sqrt{Var\left[u^{(l)}\right]}>0$. For every activation $\hat{u}^{(l)}$, the shifting and scaling parameters are paired $\beta^{(l)}$ and $\gamma^{(l)}$, shift and scale the normalized value by,

$$v = \gamma^{(l)}\hat{u}^{(l)} + \beta^{(k)} \tag{6}$$

The above parameters are action done backpropagation. The novel activation, $u^{(l)}$ can be improved if the system studies by doing the following setting for the backpropagation.

$$\gamma^{(l)} = \sqrt{Var\left[u^{(l)}\right]} \text{and } \beta^{(l)} = E\left[u^{(l)}\right] \tag{7}$$

After one or more convolutional layers, a pooling layer is usually included in the conventional CNN architecture. The pooling layer's goal is to reduce feature maps' spatial size, which in shot decreases the amount of training limits and computational difficulty. Spatial Pyramid Pooling (SPP) collects more spatial information simply by having additional spatial bins than a representative pooling process. This helps the network discern between the complex inputs. Let H and W represents the height and width of the feature map, correspondingly. Fig 5 shows the architecture of the Dilated CSPP.

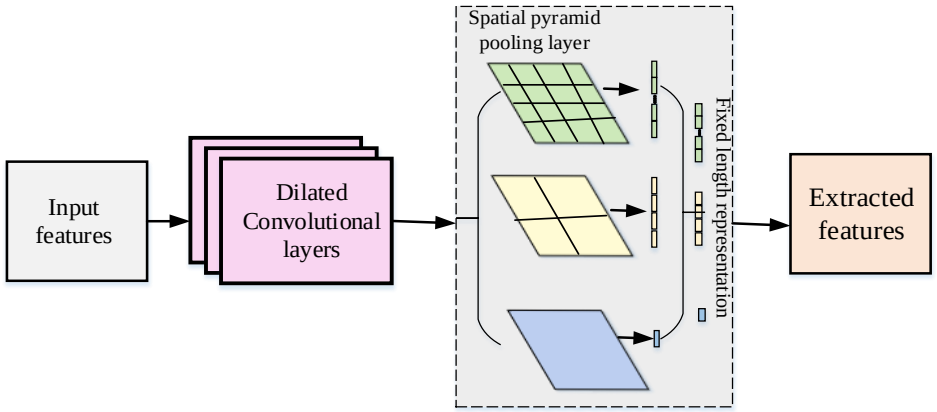

Fig. 5. Architecture of Dilated CSPP

If the grid size of SPP is $g \times g$, the size of the filter is $F = F_H = F_W$. It is designed by $F_H = \left\lceil H/g \right\rceil$ and $F_W = \left\lceil W/g \right\rceil$. For pooling, the straight height and straight width are represented as s_H and s_W separately, here, $s_H = \left\lceil H/g \right\rceil$ and

$s_W = \left[W / g \right]$. The feature map must have padding, where $pad_H = g \times s_H - H$ implies the padding for height and $pad_W = g \times s_W - W$ implies the padding for width. Let $V = 1,.....v$ represents the v-level of SPP. The $V-th$ level operation is calculated by using the below equation.

$$SPP = \sum_{V=1}^{v} g_V^2 \tag{8}$$

Here g_v is the index term for the SPP grid size, $g_V \times g_V$ and $g_V = r > 0$.

$$SPP_x = spp \times fk_L \tag{9}$$

Where SPP_x denotes total feature length produced through SPP when applied to the $L-th$ layer for the convolutional block. A 50% dropout rate is employed prior to the combined SPP features being fed into the first fully connected layer and applied similarly to the output of the first fully connected layer. In addition, batch normalization used on first layer, which is fully connected. Dropout helps prevent the system from overfitting the data by rotating off the large number of neurons asynchronously and randomly. Proposed model used dilated CSPP model for extracting multi-level scale features which combines the encoder and decoder module. Dilated CSPP model can get more receptive fields shows that resampling features of different scales is effective and can accurately and efficiently classify areas of an arbitrary scale. On the other hand, connecting the low-level and high-level multi-scale features enhances the robustness of the process, and produces competitive results in decoder part.

3.3 Feature Fusion

Using feature fusion, the features from the two parallel paths are combined form the ending set of features. The proposed method combines features using an element-wise summation [31] strategy. The element-wise summing is used to combine both of these derived features. The fusion component given in the study is constructed on a gated fusion module (GFM), which is different from standard ways for feature fusion in cross-modal stream, which typically rely on element-wise summation and concatenation operation. This section collects information depending on how helpful the associated lateral features are from the DenseSqueeze Network and the Dilated CSPP. Fig 6 represents the architecture of the element-wise summation module.

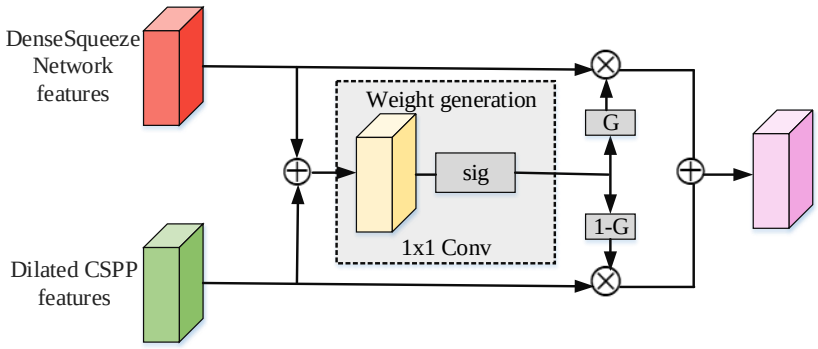

Fig. 6. Architecture of element-wise summation module.

Take F_{DS} and F_{Dcpp} are the output feature map on the DenseSqueeze Network and Dilated CSPP, respectively. The features are first concatenated to create the fused feature map f_{Fusion}. Then, the feature channels' dimension is reduced by using the convolution operation with a 1x1 kernel, w_e to determine how modalities correlate with one another. To get at least the weighed probability matrix, M the sigmoid function is used.

$$f_{Fusion} = w_e \left(F_{DS} F_{DCPP} \right) \tag{10}$$

$$M = sig\left(f_{Fusion} \right) \tag{11}$$

Where $\oplus$ represents the concatenation operation, sig denotes the sigmoid function. The gate fusion map, $f_{gate-Fusion}$ is given by,

$$\begin{aligned} f_{gate-Fusion} &= \left(F_{DS} \otimes G^{DS}\right) \oplus \left(F_{DCPP} \otimes G^{DCPP}\right) \\ &= \left(\left(F_{DS} \otimes G\right) \oplus \left(F_{DCPP} \otimes \left(1-G\right)\right)\right) \end{aligned} \tag{12}$$

Where $\otimes$ represents the Hadamard product. Let $G^{DS} = G$ and $G^{DCPP} = 1-G$ denotes the weighted matrix for DenseSqueeze Network and Dilated CSPP models.

3.4 Classification using Softmax

CNN's classification layer utilizes the Softmax classifier by default because it is the most effective and straightforward discriminatory classifier. The distinction between training and test samples is determined by the class of new features input of the testing picture using the Softmax discriminant classifier (SDC), which employs a nonlinear transformation function. The rule for traditional binary data is similar to the learning strategy used by the softmax classifier. The logistic sigmoid function is generalized into the softmax function, which can handle multiclass classification issues. The softmax classifier's mathematical expression is given in the following equation.

$$c_x\left(y\right) = \frac{n^{y_l}}{\sum_y n^{y_k}} \tag{13}$$

Where c_x represents the classification function, x denotes the $x-th$ element of the vector class scores c, natural logarithm is n, the position of any arbitrary real-valued scores in a vector denoted as y. The normalized class probabilities are calculated using Softmax as a classifier.

3.4.1 Loss function optimized using Improved Artificial Fish Swarm algorithm

The proposed method uses Improved AFS [32] to optimize the loss function in the network. The improved AFS algorithm consists of four variables $visra$ denotes the visual radius, $mstep$ represents changing the step size between iterations, the try number denoted $trynum$, and the crowd factor represents $\left(0 < delta < 1\right)$. Moreover, the AFS consists of five behaviours that are AFS-Swarm, AFS-Follow, AFS-Prey, AFS-Move and AFS-Evaluate.

3.4.1.1 AFS-Swarm-phase

This is a basic biological behaviour that causes the AF to seek out high-quality and concentrated food. The random equation for AFS is denoted as follows.

$$A_y = A_x + visra \times rand \tag{14}$$

Where A_x denotes the current state of AFS, and the randomly chosen state within the perception is A_y. Suppose B_x and B_y concentration of food for the states A_x and A_y respectively. If $B_x < B_y$ problem for the next state can expressed in the following equation.

$$A_x^{ts+1} = A_x^{ts} + \frac{A_y - A_x^{ts}}{\| A_y - A_x^{ts} \|} \times msteps \times rand \tag{15}$$

Where ts denotes the time. Otherwise, the AF will repeatedly try to find a workable solution until it exceeds the try number limit. After going over the limit, it decides to move a step at random.

$$A_x^{ts+1} = A_x^{ts} + visra \times rand \tag{16}$$

3.4.1.2 AFS-Prey phase

The current state of AFS is A_x, p_s partners in the field of current exploration $\left(d_{x,y} < visra\right)$, and A_c is the center position, while $B_c / p_s > B_x * delta$. The AF moves a little bit closer to its partners' center position.

$$A_x^{ts+1} = A_x^{ts} + \frac{A_c - A_c^{ts}}{\| A_c - A_x^{ts}} \times msteps \times rand \tag{17}$$

If not, the AF engages in its preying behaviour.

3.4.1.3 AF-Follow

When a fish or group of fish finds a food supply, the other fish in the area swim quickly to follow them, which can tempt other fish to join the queue. The number of companions inside their current exploration field $\left(d_{x,y} < visra\right)$ is p_s. Between the partners, A_y the highest level of fitness is denoted as B_y. If $B_y / p_s > B_y * delta$, it also indicates that there is still more food available and that A_y is not in a very congested area. As a result, the AF moves closer to its ideal partner.

$$A_x^{ts+1} = A_x^{ts} + \frac{A_y - A_x^{ts}}{\| A_y - A_x^{ts}} \times msteps \times rand \tag{18}$$

If not, the AF engages in its preying behaviour.

3.4.1.4 AF-Move

The movement behaviour complements and simplifies the prey behaviour. The AF goes in any direction, then chooses a random state from the vision and moves in that direction.

$$A_x^{ts+1} = A_x^{ts} + visra \times rand \tag{19}$$

In this work, two improvement strategies have been proposed to address the existing shortcomings and enhance the AFS performance. One relates to AFS's parameters $\left(visra \ and \ msteps\right)$, and the other to the AFS-Prey model's structure. The steps for the Improved AFS are discussed below.

3.4.1.5 The Self-Adaptive Factor

The *visra* and $mstep$ are fixed in the original AFS, which results in a slow convergence and a low-quality solution. In addition, the experiments show that fixed following behaviour and swarming behaviour are generated to obtain a large value of p_s because the number of iterations rises, and the distance between the fellows and the AFS becomes very small. The $visra_{\min}$ is configured to ensure the effectiveness of the late search procedure.

$$visra = \exp\left(-1 \times \left(M / visra_{\max}\right)\right) \times d_{x,y} + visra_{\min} \tag{20}$$

Here M denotes the Self-Adaptive Factor. The $visra$ performance and $mstep$ performance of the AFS appear to be mutually independent; they are closely related.

$$msteps = ran \times visra + msteps_{\min} \tag{21}$$

3.4.1.6 Improves AFS-Prey

The typical preying behaviour enables the AF to randomly hunt areas in its field of view with high food consistencies, but this is time-consuming and inefficient. An improved AFS-Prey model that incorporates the global optimization solution (GOS) into the preying behavior is described here in order to overcome this problem. The Gbest is used by the upgraded AFS-Prey model to guide AFS exploration, and the present condition is represented by A_x, and B_M representing the value of food consistency (fitness) in the state of A_M.

$$A_M = A_x + \frac{GOA - A_x}{\| GOA - A_x \|} \times rand \times msteps \tag{22}$$

If $B_k > B_x$ the formula below can be used to determine A_i subsequent state.

$$A_x^{ts+1} = A_M \tag{23}$$

If not, the AF keeps randomly scanning its range of vision, mimicking a predator's natural behaviour. Fig 7 shows the flowchart for the Improved AFS.

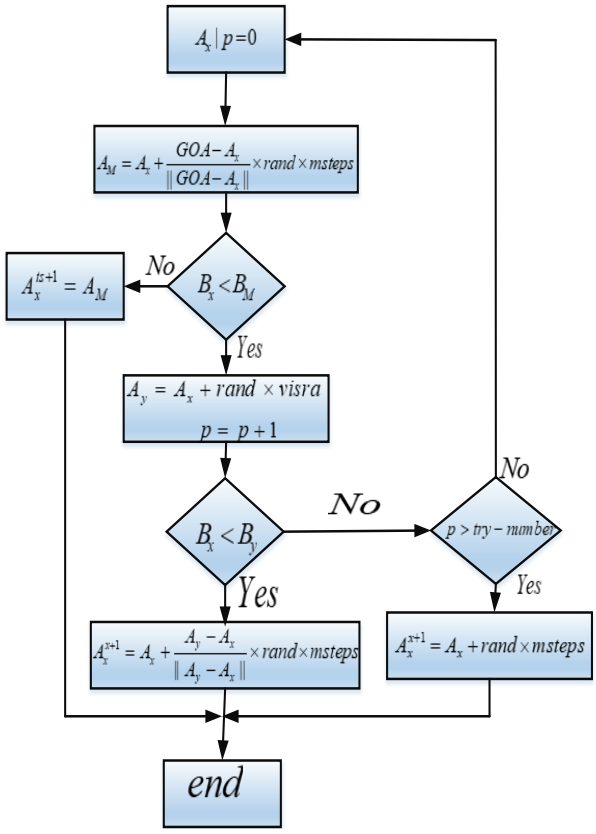

Fig. 7. Flowchart of proposed Improved AFS

The modified AFS-Prey model guarantees the traversability of the algorithm and additionally improves the effectiveness in finding the global optimal solution. By using the softmax classifier in the last layer and using an improved AFS algorithm to optimize losses in the network model, AML classification is carried out effectively.

4. Results and Discussion

In this section, the various experimental studies for existing methods and proposed methods are defined. In this section, various performance metrics are analyzed and compared with other existing systems. The proposed method uses the AML-Cytomorphology_LMU dataset, which is used to classify AML. Various performance metrics such as Accuracy, Precision, F-Score, Area under the Curve (AUC), True Positive Rate (TPR), True Negative Rate (TNR), False Positive Rate (FPR) and False Negative Rate (FNR) are measured for the AML-Cytomorphology_LMU dataset. These performance metrics are analyzed for various existing systems such as FCL, SVM, XGBoost, RF, CNN, ResNet-34, ResNeXt-50 and VGG-19. These performances are analyzed and compared with various existing and proposed methods discussed in this section. Hyper parameter description for proposed model is shown in Table 2.

Table 2. Hyper parameter details

Hyper-parameters	Values
Number of epochs	300
Number of dense layer	6
Batch Size	32
first, second, third, fourth, fifth, sixth dense layer	512,256,128,64,32,4
Activation function of first five dense layer	RELU
Activation function of final dense layer	softmax
Optimizer	Improved AFS optimization
Learning rate	0.01
Loss function	categorical cross entropy

4.1 Dataset description

From 2014 to 2017, the Munich AML morphology database contained 18,365 single-cell pictures from 100 patients with AML at the University Hospital of Munich, as well as 100 individuals with no evident hematological malignancy. These photos are from peripheral blood smears. Images were taken with an M8 digital microscope and scanner (Precipoint GmbH, Freising, Germany) while immersed in oil and magnified 100 times. Pathological and non-pathological leukocytes have been classified using a common morphological categorization system devised by trained clinical practitioners. To assess inter- and intra-rater variability, a subset of photos was re-annotated up to two times.

4.2 Performance Measures

Based on the evaluation of existing AML classification methods, the proposed work is completed by adopting many methods in terms of accuracy, precision, F-score, AUC, TPR, TNR, FPR, and FNR.

4.2.1 Accuracy

The ratio of the overall number of right estimates to the total number of predictions is known as accuracy.

$$ACC = \frac{NTN + NTP}{NTP + NFP + NFN + NTN} \tag{24}$$

Here NTP, NFP, NFN, NTN denotes the number of true positives, false positives, false negatives, and true negatives, respectively.

4.2.2 Precision

Precision is referred to as the positive predictive value. The precision is calculated using the below equation,

$$PRE = \frac{NTP}{NTP + NFP} \tag{25}$$

4.2.3 F-score

F-score trade-off values between recall and precision, which consider NFP and NFN. It measures the overall accuracy of an ML model, and it can be expressed in the below equation.

$$F - Score = \frac{2 \times pre \times rec}{pre + rec} \tag{26}$$

4.2.4 TPR

TPR refers to the possibility that a test result will actually be positive. TPR is calculated using the following equation.

$$TPR = \frac{NTP}{NFN} \tag{27}$$

4.2.5 TNR

The TNR is called the proportionality of negative values across many instances. TNR is calculated using the following formula,

$$TNR = \frac{NTN}{NTN + NFP} \tag{28}$$

4.2.6 FPR

The FPR is calculated by dividing the total number of false positives by the total number of true negatives. The following equation is used to determine the FPR.

$$FPR = NFP / (NFP / NTN) \tag{29}$$

4.2.7 FNR

FNR represents the proportion of affirmative test outcomes that yield negative results. The FNR is calculated using the following equation.

$$FNR = NFN / (NTP / NFN) \tag{30}$$

4.3 Performance analysis

Performance is analyzed for existing and proposed methods based on the AML-Cytomorphology_LMU dataset. Fig 8 shows the performance comparison of accuracy.

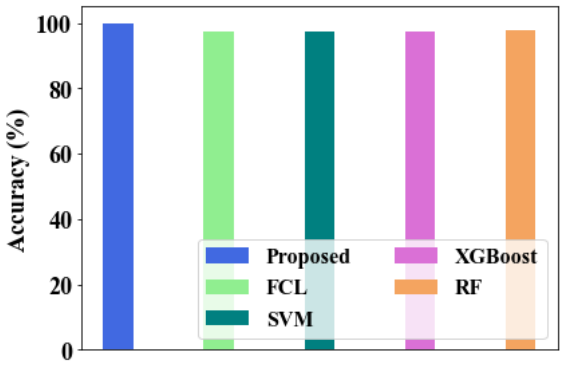

Fig. 8. Performance comparison of accuracy parameter

Fig 8, compares the proposed model with the various existing methods, such as Full Container Load (FCL), Support Vector Machine (SVM), XGBoost and Random Forest (RF) using the AML Cytomorphology_LMU dataset. The proposed model achieves better performance than other existing methods. An accuracy of 99% was achieved with the proposed method using the AML-Cytomorphology_LMU dataset. The existing models can achieve lower accuracy because it takes more time to calculate problems. Fig 9 shows the performance comparison of precision, F-score and AUC parameters.

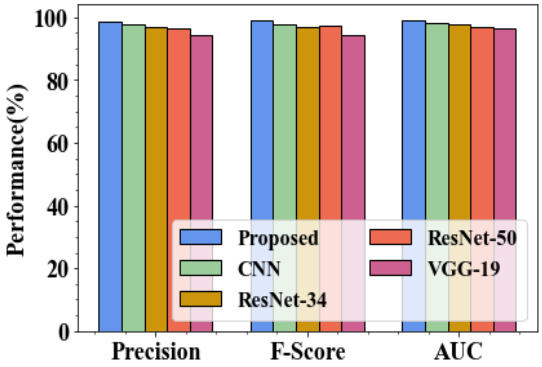

Fig. 9. Comparison of Precision, F-score and AUC parameters.

Figure 9 compares the proposed model with the various existing methods, such as CNN, ResNet-34, ResNet-50 and VGG-19. The proposed model achieved better results in terms of 98.5% precision, 98.9% F-score and 99% AUC. The existing models may achieve lower performance compared to the proposed model. Fig 10 shows the performance comparison of TPR and TNR.

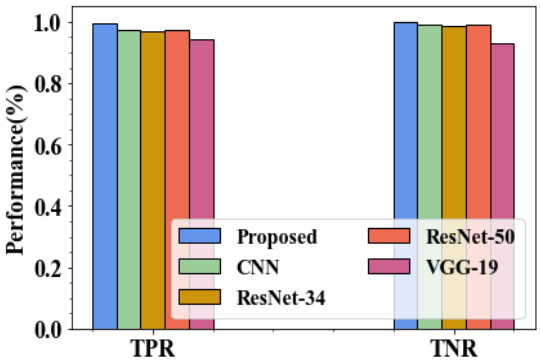

Fig. 10. Performance of TPR and TNR parameter

Figure 10 compares the proposed model with the various existing methods, such as CNN, ResNet-34, ResNet-50 and VGG-19. The proposed model achieved better results in terms of 98.2% TPR and 99.1% TNR. The existing models may achieve lower performance compared to the proposed model. Fig 11 shows the performance comparison of FPR and FNR.

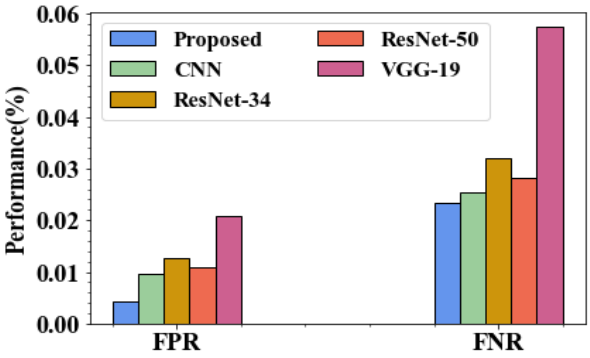

Fig. 11. Performance of FPR and FNR parameter

Fig 11 compares the proposed model with the various existing methods, such as CNN, ResNet-34, ResNet-50 and VGG-19. The proposed model achieved a lower result in terms of 0.0071 in FPR and 0.0234 in FNR. The existing model achieves more results in terms of FPR and FNR compared to the proposed model. Fig 12 shows the performance of the computation time.

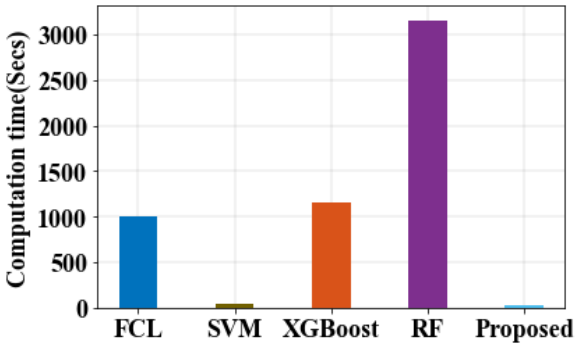

Fig. 12. Performance comparison of computation time

Fig 12 compares the proposed model with the various existing methods, such as FCL, SVM, XGBoost and RF, using the AML-Cytomorphology_LMU dataset. The computation time of a proposed model offers less running time than other existing models. The computing time of a proposed model is 25.1 seconds, while the existing model takes more than 25.1 seconds. Fig 13 (a) and (b) shows the performance of the proposed accuracy and loss curve.

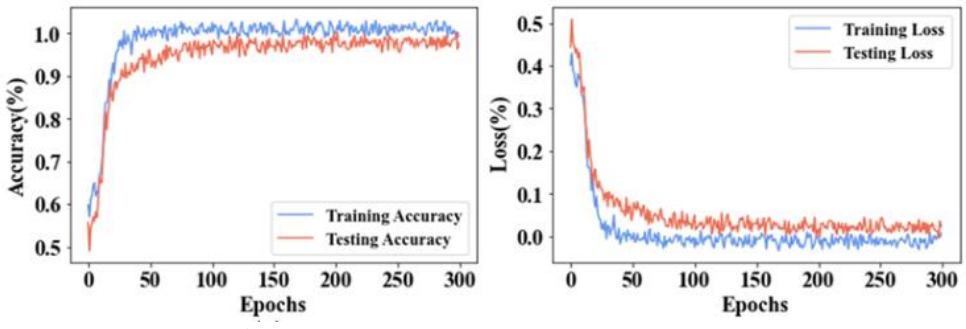

Fig. 13. Training and Testing measures (a) Accuracy (b) Loss

The proposed method is observed during training and testing using an accuracy and loss graph with 300 epochs. Here, the loss function is considered cross-entropy for the training and testing phases to find the accuracy and loss of the proposed model. When comparing training and testing accuracy, small changes in accuracy rates are observed. Due

to the efficient introduction of the proposed technique and effective training, the proposed classification model has a lower error value. Fig 14 shows the confusion matrix for the proposed model.

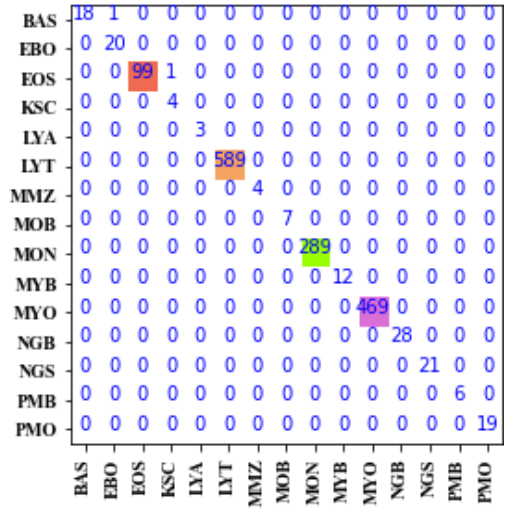

Fig. 14. Confusion matrix for AML-Cytomorphology_LMU dataset

In Fig 14, the confusion matrix is evaluated for several classes present in the dataset, namely the Basophil (BAS), Erythroblast (EBO), Eosinophil (EOS), Smudge cell (KSC), Lymphocyte atypical (LYA), Lymphocyte typical (LYT), Metamyelocyte (MMZ), Monoblast (MOB), Monocyte (MON), Myelocyte (MYB), Myeloblast (MYO), Neutrophil band (NGB), Neutrophil segmented (NGS), Promyelocyte bilobled (PMB), and Promyelocyte (PMO) classes. The proposed model can make more accurate predictions than other existing models. The proposed model can predict the classes represented as numbers based on the AML-Cytomorphology_LMU dataset. Thus, the proposed model can obtain a more efficient AML classification model. Fig 15 shows the scatterplot of the AML-Cytomorphology_LMU dataset.

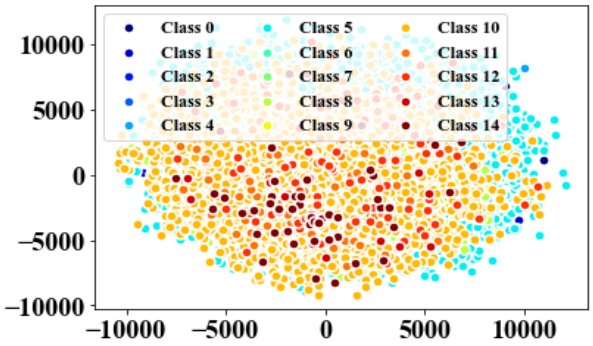

Fig. 15. Scatter plot of AML-Cytomorphology_LMU dataset

The scatter plot illustration illustrates the values of two numeric variables through the use of points. For each data point, its value is represented by its position along the horizontal and vertical axis. It is possible to illustrate the relationships between variables using scatter graphs. The ablation study for the proposed model is described in Table 3.

Table 3. Ablation study for accuracy of the proposed model

Performance	Without noise filtering (%)	Without image resizing (%)	Without colour conversion (%)	Without multi-level dense feature extraction (%)	Without multi-level scale feature extraction (%)	Proposed (%)
Accuracy	96.52	96.99	97.43	98	98.12	**99**
Precision	94.99	95.1	95.17	95.21	96.54	**98.5**
F-Score	95	95.91	96.28	97.17	97.98	**98.9**
AUC	93.67	95.32	96.43	98.12	98.74	**99**

In this study, the AML-Cytomorphology_LMU dataset is used for the classification process. For without noise filtering, the proposed method attain less performance values in terms of 96.52% accuracy, 94.99% precision, 95% F-score and 93.67% AUC. Without filtering noises the input image contain unwanted noises that produce miss

classification results and less performance. Without image resizing the proposed model attain 96.99% accuracy, 95.1% precision, 95.91% F-score and 95.32% AUC performance results. Without image resizing the image contain big size of file its lead to take complex process and produce low performance results. Without colour conversion proposed method attain 97.43% accuracy, 95.17% precision, 96.28% F1-score and 95.32% AUC results. Without CMYK colour conversion, image face issues in difficulty of disease portion identification it may lead to produce misclassification results. Without multilevel dense and scale feature extraction proposed approach attain 98% and 98.12% accuracy, 95.21% and 96.54% precision, 97.17% and 97.98%F-score and 98.12% and 98.74% AUC. Without feature extraction the image contain all set of features its lead to increase the complexity of the model, that fore, proposed model attain low performance values. Finally by using proposed noise filtering, image resizing and colour conversion, and feature extraction techniques the proposed approach produce high classification results which is 99% accuracy, 98.5% precision, 98.9% F-score and 99% AUC. Table 4 shows the computational cost and the network scale for the various existing and proposed models.

Table 4. Computational cost and the network scale

Models	Parameters	FLOPs(G)
CNN	7.397	1.380
ResNet-34	21.288	3.761
ResNet-50	22.992	4.257
VGG-19	139.595	19.634
Proposed	**6.405**	**1.222**

The proposed model has a small number of parameters but delivers the best performance on all remaining metrics. Compared with the existing model, the proposed model has a small number of parameters, namely 6,405, and the existing models are more than 7. In contrast, the proposed model has the fewest network parameters and requires the least amount of computing work. The proposed model focuses on decreasing the tunable hyper-parameters, which in turn reduces the computational complexity and memory overhead of the produced model. A minimal number of convolution and de-convolution layers are used in the proposed model. Hence, the computational complexity of the proposed model is very less as compared to all other models. Fig 16 shows the classification results.

Fig 16 shows initial improvements made to a collection of image samples collected from the AML Cytomorphology_LMU dataset. The collected image samples are filtered with NGF; then, the RoI is identified using the IML technique. Each RoI image is used to predict the AML classes.

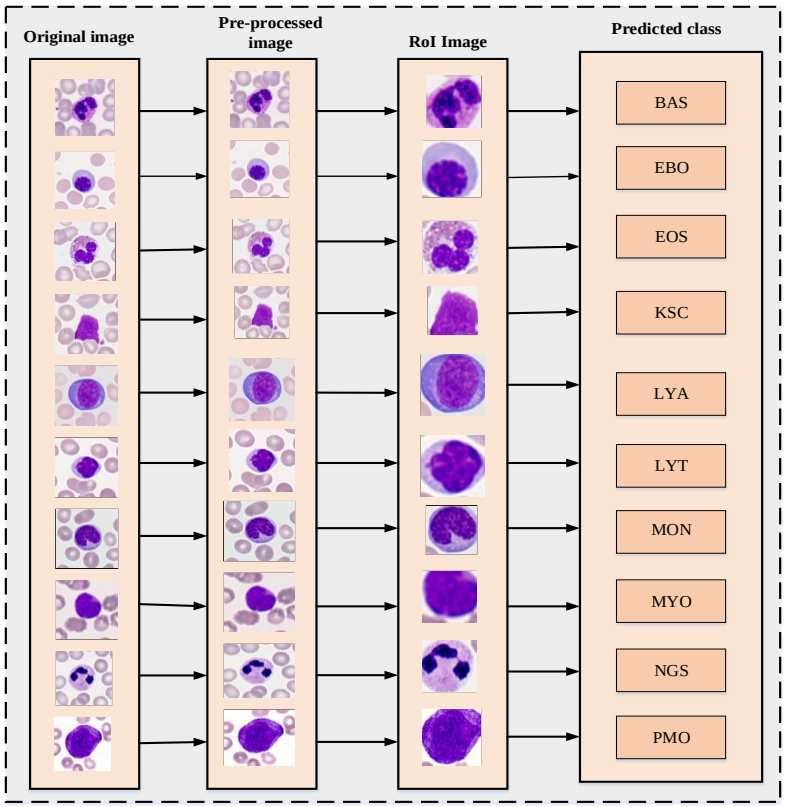

Fig.16. Classification of outcomes

4.4 Discussion

The main aim of the proposed model is automatic AML detection and classification of several classes of AML. The research methodology is performed on peripheral blood spot images, this images provide help in early detection of AML disease. Compare to existing AML classification methods proposed model used three pre-processing stage. Firstly, NGF is used to remove the unwanted noises in input images. Secondly filtered image resized to a standard sized. Third, the resized RGB image is converted into CMYK colour space to perform colors conversion. Compare to single pre-processing method three proposed pre-processing techniques may helpful to produce good quality image and better detection of AML. Colour conversion image is fed into IML for the identification of RoI. RoI makes a boundaries to identify disease portions on the image. After identification RoI features are extracted, here two techniques are used to extract multi-level dense and multi-level scale features. DenseSqueeze network is used to extract the multi-level dense features. DenseSqueeze networks combines the benefits of Dense and Squeeze networks. DenseNet reuse feature map through dense connection, reusing feature maps from various layers to decrease interdependence between layers. Squeeze network make a balance between accuracy and computational time. Squeeze block in DenseSqueeze network contain the dilated convolutional layer, this is one of the novelty. The dilated convolutional block reduce the parameter of the model and network scale. Multi-level scale features from AML disease are extracted using Dilated CSPP model and then the decoder is used to capture the clear boundary of image. On the other hand, connecting the low-level features and high-level features enhances the robustness of the algorithm, and produces competitive results in decoder part. Multi-level dense and scale features are merged using element-wise summation, here GFM module is used to perform element-wise summation process.

Finally, the AML classification is performed by using softmax classifier to classify various classes of AML disease. Improved AFS algorithm is used to optimize the network loss and hyper parameter tuning. Here the AFS algorithm is improved by using self-adaptive visual, moving step, and new scheme of the preying behavior. Overall novelty of the proposed model is accurate classification of AML, produce less complex model, and reduce misclassification and detection time. Through the evaluation of the proposed method, it can be obvious that the limitations of the existing methods can be effectively overcome. In [21] and [25] the limitation is less features, but the proposed method used multi-level scale and dense features. Here the two feature extraction technique is used namely DenseSqueeze and Dilated CSPP models for extracting multi-level scale and dense features respectively. In [22] the limitation is simple and basic techniques are used, but the proposed model used advanced techniques and produce efficient results in AML classification. In [24] the limitation is less performance model, but proposed model achieves high performance results compare to other model that are described in results section. In [24] the limitation is can't detect types of AML, but the proposed model but the proposed model detect 14 classes of AML disease. In [25], the limitation is high complex model but the proposed model have less complexity.

5. Conclusion

This work presents a computer-assisted deep learning model-based AML classification from peripheral blood spot images, which is helpful in earlier AML diagnosis. First, the input image is pre-processed, which includes noise filtering, image resizing, and colour conversion. The noise in the image is filtered using NGF. It then resizes the image to a standard size and converts the RGB image to the CMYK colour space. The RoI is then identified using the IML technique. Next, the valuable multi-level dense features are extracted using the DenseSqueeze network, and the multi-scale features are extracted using the Dilated CSPP. These two extracted features are merged using element-wise summation. Finally, the softmax classifier is used in the last layer to classify the AML classes and the loss in the network is optimized using the improved AFS algorithm. The proposed work achieved 99% accuracy, 98.5% precision, and 98.9% F-score using the AML-Cytomorphology_LMU dataset. In the future, a hybrid optimization approach could be used to predict the optimal solution for accurate classification with fewer classification errors, and more data sets would also be considered.

References

[1] Papaemmanuil, Elli, Moritz Gerstung, Lars Bullinger, Verena I. Gaidzik, Peter Paschka, Nicola D. Roberts, Nicola E. Potter et al. "Genomic classification and prognosis in acute myeloid leukemia." *New England Journal of Medicine* 374, no. 23 (2016): 2209-2221.

[2] Arber, Daniel A. "The 2016 WHO classification of acute myeloid leukemia: What the practicing clinician needs to know." In *Seminars in hematology*, vol. 56, no. 2, pp. 90-95. WB Saunders, 2019.

[3] Arber, Daniel A. "Acute myeloid leukemia." In *Hematopathology*, pp. 429-466. Elsevier, 2018.

[4] Yohe, Sophia. "Molecular genetic markers in acute myeloid leukemia." *Journal of clinical medicine* 4, no. 3 (2015): 460-478.

[5] Hong, Ming, and Guangsheng He. "2016 Revision to the WHO classification of acute myeloid leukemia." *Journal of Translational Internal Medicine* 5, no. 2 (2017): 69-71.

[6] Devillier, Raynier, Véronique Mansat-De Mas, Veronique Gelsi-Boyer, Cecile Demur, Anne Murati, Jill Corre, Thomas Prebet et al. "Role of ASXL1 and TP53 mutations in the molecular classification and prognosis of acute myeloid leukemias with myelodysplasia-related changes." *Oncotarget* 6, no. 10 (2015): 8388.

[7] Vardiman, James, and Kaaren Reichard. "Acute myeloid leukemia with myelodysplasia-related changes." *American Journal of Clinical Pathology* 144, no. 1 (2015): 29-43.

[8] Boddu, Prajwal C., Tapan M. Kadia, Guillermo Garcia‐Manero, Jorge Cortes, Mansour Alfayez, Gautam Borthakur, Marina Konopleva et al. "Validation of the 2017 European LeukemiaNet classification for acute myeloid leukemia with NPM1 and FLT3‐internal tandem duplication genotypes." *Cancer* 125, no. 7 (2019): 1091-1100.

[9] Yao, Jianfeng, Guixin Zhang, Chen Liang, Gang Li, Xin Chen, Qiaoling Ma, Weihua Zhai et al. "Combination of cytogenetic classification and MRD status correlates with outcome of autologous versus allogeneic stem cell transplantation in adults with primary acute myeloid leukemia in first remission." *Leukemia research* 55 (2017): 97-104.

[10] Thanh, T. T. P., Caleb Vununu, Sukhrob Atoev, Suk-Hwan Lee, and Ki-Ryong Kwon. "Leukemia blood cell image classification using convolutional neural network." *International journal of computer theory and engineering* 10, no. 2 (2018): 54-58.

[11] Weinberg, Olga K., Christopher J. Gibson, Traci M. Blonquist, Donna Neuberg, Olga Pozdnyakova, Frank Kuo, Benjamin L. Ebert, and Robert P. Hasserjian. "Association of mutations with morphological dysplasia in de novo acute myeloid leukemia without 2016 WHO Classification-defined cytogenetic abnormalities." *haematologica* 103, no. 4 (2018): 626.

[12] Maiti, Abhishek, Wei Qiao, Koji Sasaki, Farhad Ravandi, Tapan M. Kadia, Elias J. Jabbour, Naval G. Daver et al. "Venetoclax with decitabine vs intensive chemotherapy in acute myeloid leukemia: a propensity score matched analysis stratified by risk of treatment‐related mortality." *American journal of hematology* 96, no. 3 (2021): 282-291.

[13] Martelli, Alberto M., Francesca Paganelli, Antonietta Fazio, Chiara Bazzichetto, Fabiana Conciatori, and James A. McCubrey. "The key roles of PTEN in T-cell acute lymphoblastic leukemia development, progression, and therapeutic response." *Cancers* 11, no. 5 (2019): 629.

[14] Arber, Daniel A., Attilio Orazi, Robert Hasserjian, Jürgen Thiele, Michael J. Borowitz, Michelle M. Le Beau, Clara D. Bloomfield, Mario Cazzola, and James W. Vardiman. "The 2016 revision to the World Health Organization classification of myeloid neoplasms and acute leukemia." *Blood, The Journal of the American Society of Hematology* 127, no. 20 (2016): 2391-2405.

[15] Wang, M., J. Lindberg, D. Klevebring, C. Nilsson, A. S. Mer, M. Rantalainen, Sören Lehmann, and H. Grönberg. "Validation of risk stratification models in acute myeloid leukemia using sequencing-based molecular profiling." *Leukemia* 31, no. 10 (2017): 2029-2036.

[16] Weinberg, Olga K., Aliyah R. Sohani, Parul Bhargava, and Valentina Nardi. "Diagnostic work‐up of acute myeloid leukemia." *American journal of hematology* 92, no. 3 (2017): 317-321.

[17] de Noronha, Thiago Rodrigo, Miguel Mitne-Neto, and Maria de Lourdes Chauffaille. "Mutational profiling of acute myeloid leukemia with normal cytogenetics in Brazilian patients: the value of next-generation sequencing for genomic classification." *Journal of Investigative Medicine* 65, no. 8 (2017): 1155-1158.

[18] Rawat, Jyoti, Annapurna Singh, H. S. Bhadauria, Jitendra Virmani, and Jagtar Singh Devgun. "Computer assisted classification framework for prediction of acute lymphoblastic and acute myeloblastic leukemia." *Biocybernetics and Biomedical Engineering* 37, no. 4 (2017): 637-654.

[19] Khan, Maliha, Rabbia Siddiqi, and Kiran Naqvi. "An update on classification, genetics, and clinical approach to mixed phenotype acute leukemia (MPAL)." *Annals of hematology* 97 (2018): 945-953.

[20] Yang, John J., Tae Sung Park, and Thomas SK Wan. "Recurrent cytogenetic abnormalities in acute myeloid leukemia." *Cancer Cytogenetics: Methods and Protocols* (2017): 223-245.

[21] Alagu, S., and K. Bhoopathy Bagan. "Computer assisted classification framework for detection of acute myeloid leukemia in peripheral blood smear images." In *Innovations in Computational Intelligence and Computer Vision: Proceedings of ICICV 2020*, pp. 403-410. Springer Singapore, 2021.

[22] Yoshifuji, Kota, Takashi Toya, Noriyo Yanagawa, Fumikazu Sakai, Akihito Nagata, Noritaka Sekiya, Kazuteru Ohashi, and Noriko Doki. "CT classification of acute myeloid leukemia with pulmonary infiltration." *Japanese Journal of Radiology* 39, no. 11 (2021): 1049-1058.

[23] Sha, K., Y. Lu, P. Zhang, R. Pei, X. Shi, Z. Fan, and L. Chen. "Identifying a novel 5-gene signature predicting clinical outcomes in acute myeloid leukemia." *Clinical and Translational Oncology* 23 (2021): 648-656.

[24] Bukhari, Maryam, Sadaf Yasmin, Saima Sammad, Abd El-Latif, and A. Ahmed. "A deep learning framework for leukemia cancer detection in microscopic blood samples using squeeze and excitation learning." *Mathematical Problems in Engineering* 2022 (2022).

[25] Granero, Marco Aurélio, Cristhian Xavier Hernández, and Marcos Eduardo Valle. "Quaternion-valued convolutional neural network applied for acute lymphoblastic leukemia diagnosis." In *Brazilian conference on intelligent systems*, pp. 280-293. Cham: Springer International Publishing, 2021.

[26] Boldú, Laura, Anna Merino, Andrea Acevedo, Angel Molina, and Jose Rodellar. "A deep learning model (ALNet) for the diagnosis of acute leukaemia lineage using peripheral blood cell images." *Computer Methods and Programs in Biomedicine* 202 (2021): 105999.

[27] Sathish, Dayakshini, Surekha Kamath, Keerthana Prasad, and Rajagopal Kadavigere. "Role of normalization of breast thermogram images and automatic classification of breast cancer." *The Visual Computer* 35 (2019): 57-70.

[28] Xu, Yang, Shiyin Wei, Yuequan Bao, and Hui Li. "Automatic seismic damage identification of reinforced concrete columns from images by a region‐based deep convolutional neural network." *Structural Control and Health Monitoring* 26, no. 3 (2019): e2313.

[29] Zhang, Yiming, Na Qin, Deqing Huang, Bi Wu, and Ziyi Liu. "High-accuracy and adaptive fault diagnosis of high-speed train bogie using dense-squeeze network." *IEEE Transactions on Vehicular Technology* 71, no. 3 (2022): 2501-2510.

[30] Geng, Lei, Jia Wang, Zhitao Xiao, Jun Tong, Fang Zhang, and Jun Wu. "Encoder-decoder with dense dilated spatial pyramid pooling for prostate MR images segmentation." *Computer Assisted Surgery* 24, no. sup2 (2019): 13-19.

[31] Li, Junxia, Zefeng Pan, Qingshan Liu, and Ziyang Wang. "Stacked U-shape network with channel-wise attention for salient object detection." *IEEE Transactions on Multimedia* 23 (2020): 1397-1409.

[32] Xu, Han, YouQun Zhao, Chao Ye, and Fen Lin. "Integrated optimization for mechanical elastic wheel and suspension based on an improved artificial fish swarm algorithm." *Advances in Engineering Software* 137 (2019): 102722.

Authors' Profiles

Mr Krishna Prasad Palli is an engineering educator since 2008 and a Researcher in Computer Science and Engineering, Vasireddy Venkatadri Institute of Technology, JNTUK. He did M.Tech from Acharya Nagarjuna University in Computer Science and Engineering. He is interested in Digital Image Processing, Machine Learning and Deep Learning domains.

Dr. Edara Sreenivasa Reddy is a Professor & Dean R&D of Dr YSR University College of Engineering of Acharya Nagarjuna University. He did Master of Technology in Computer Science Engineering from Sir Mokhsagundam Visweswariah University, Bangalore. He also did Mater of Science from Birla Institute of Technological Sciences, Pilani. He did Philosophical Doctorate in Computer Science Engineering from Acharya Nagarjuna University, Guntur. Prof.E.S.Reddy, guided successfully more than twenty five research scholars for PhD degree. His research areas of interest are in various domains including Digital Image Processing.

Dr Chandra Sekharaiah K. is a Professor Computer Science and Engineering of JNTU, Hyderabad. In his 27 Years of experience, he served in various capacities in teaching, institutional administration and system administration. He did his Ph.D from IIT Madras and later PostDoc from University of Jyvaskyla, Finland. After B.Tech., M.Tech., Ph.D. and PostDoc., He has 100 plus or minus research publications in various National and International Conferences and Journals. Dr Chandra Sekharaiah guided many research scholars for Ph D Degree. His research interests are in the realms of modeling, engineering and understanding of software systems related to distributed, security, language engineering, databases, wireless networks, web services, cognitive informatics and computer ergonomics domains of computing.

How to cite this paper: Krishna Prasad Palli, Edara Sreenivasa Reddy, Chandra Sekharaiah K., "Computerized Acute Myeloid Leukemia Classification Using Hybrid Dilated DenseSqueeze Network from Peripheral B Stain Analysis", International Journal of Image, Graphics and Signal Processing(IJIGSP), Vol.16, No.4, pp. 87-105, 2024. DOI:10.5815/ijigsp.2024.04.07